

HIGH TEMPERATURE FLOW AND DYNAMIC RECRYSTALLIZATION IN CARRARA MARBLE

S.M. SCHMID *, M.S. PATERSON and J.N. BOLAND **

*Research School of Earth Sciences, Australian National University, Canberra A.C.T.
(Australia)*

(Received February 2, 1979; accepted for publication May 15, 1979)

ABSTRACT

Schmid, S.M., Paterson, M.S. and Boland, J.N., 1980. High temperature flow and dynamic recrystallization in Carrara marble. *Tectonophysics*, 65: 245–280.

Specimens of Carrara marble have been experimentally deformed at temperatures between 600° and 1050° and at strain rates between 10⁻² and 10⁻⁶ sec⁻¹. No single empirical flow law could be found for the whole range of experimental conditions covered. Instead it was found that three deformation regimes, each with its characteristic microstructural imprint, can be established. Above 1000 bar differential stress a relatively low strain rate sensitivity of the flow stress is observed and twinning is predominant (regime 1). Regime 2 extends down to 200 bar flow stress and exhibits the unusually high stress exponent $n = 7-8$ in the power law creep equation earlier found by Heard and Raleigh (1972) in Yule marble. The original grains exhibit a "core and mantle" structure. Only in regime 3 below 200 bar differential stress does one find lower values for n of around 4, and now a mosaic of equi-axed subgrains occupies entire grains.

Extensive recrystallization and grain boundary migration was found at the higher temperatures. The grain size produced by dynamic in-situ recrystallization was found to be inversely proportional to the applied flow stress. Scanning electron microscopy observations on split cylinders suggests substantial amounts of grain boundary sliding in the low stress region. The unusually high dislocation densities at low flow stresses as measured under the transmission electron microscope are interpreted to arise through strains induced during cooling under pressure after the deformation experiment.

In view of the fact that the different calcite rocks so far investigated under elevated temperatures and low flow stresses exhibit rather different flow laws, caution is indicated when extrapolating such empirical flow laws to geological conditions. The size of dynamically recrystallized grains may directly lead to a paleostress estimate at the time of recrystallization. A subsequent work softening effect through a change in mechanism induced by syntectonic recrystallization may play an important role in the formation of shear zones and mylonite layers.

INTRODUCTION

The study of rock deformation in experiment and in nature continues to reveal more and more complex behaviour in various rocks but, at the same

* Now at Geologisches Institut der ETH, Zürich (Switzerland).

** Now at Department of Geology, Rijksuniversiteit, Utrecht (The Netherlands).

time, it is becoming clearer which are the important variables. Thus, grain size has emerged recently as a very important variable influencing the flow of rocks at relatively high temperatures and low stresses and strain rates, in regimes that are of likely relevance in geology.

A striking example of the role of grain size is seen in Solnhofen limestone above 500°C (Schmid et al., 1977). In the fine-grained Solnhofen limestone, below a certain stress threshold that depends on temperature (1000 bars at 600°C, 300 bars at 900°C), there is a marked change in flow behaviour. The strain-rate sensitivity of the flow stress increases, grain-boundary sliding begins to make a major contribution to the strain, and the flow rate becomes markedly sensitive to grain size. Such a "superplastic" regime of flow was not observed in the coarser-grained Yule marble by Heard and Raleigh (1972) in a study up to 800°C. However, a comparison shows that the Solnhofen limestone in its superplastic regime is much weaker and more strain-rate sensitive than Yule marble at corresponding temperatures and strain rates.

It therefore became of interest to extend the study of marble to more extreme conditions to see whether a more strain-rate sensitive regime of flow is found in it also and to observe any corresponding microstructural evidence for change in the mechanism of flow. Carrara marble was chosen for this study because of its ready availability, its isotropy and suitable grain size (200 μm), and the existence of a previous study up to 500°C (Rutter, 1974).

A more strain-rate sensitive mode of flow than previously observed in marble has indeed been found to occur at higher temperatures and lower strain rates although it will be shown to have different properties from the superplastic flow in Solnhofen limestone. Also of special interest has been the observation of extensive syndeformational or dynamic recrystallization leading to a new grain size in equilibrium with the steady state flow stress. The possible relationship between such an equilibrium grain size (or subgrain size) and its application for determining the magnitude of tectonic stresses has recently become of considerable interest (Kohlstedt et al., 1976; Mercier et al., 1977; Twiss, 1977).

EXPERIMENTAL PROCEDURES

Cylindrical specimens 10 mm diameter and 20 mm length were diamond core-drilled from a single block of Carrara marble. They were then deformed in compression while under 3 kbar confining pressure at the desired temperature, using a gas-medium apparatus (Paterson, 1970, 1977). The specimens were sealed in copper jackets of 0.25 mm wall thickness during deformation. The experimental and data reduction procedures were as described in Schmid et al. (1977).

Three types of tests were used:

(1) *Constant strain rate tests.* Actually these tests were performed at constant drive motor speed but, since a constant flow stress was soon established

in most cases, the main part of the test was at a constant strain rate. These tests provided the specimens for the microstructural studies described later.

(2) *Stepping tests*. In these, the strain rate was changed abruptly at a stage well after the specimen had settled down to a constant flow stress at the initial strain rate. After a short transient strain, less than 0.1%, a new higher or lower constant flow stress was attained corresponding to the new strain rate. In some cases, a sequence of such steps in strain rate was imposed and it was found that when the original strain rate was regained the flow stress returned to a level indistinguishable from its original level, within normal scatter.

(3) *Relaxation tests*. At the end of some of the experiments a stress relaxation test was carried out in which the rate of stress was determined as a function of stress after stopping the machine drive mechanism. Ideally in such a test the strain rate at a given instantaneous value of the stress is given by the relation $de/dt = K d\sigma/dt$, where e is the non-elastic part of the total strain in the specimen and K is the elastic compliance of the relaxing system (Schmid, 1976). In practice, K consists of the sum of the compliances of the specimen and of those parts of the loading apparatus between the specimen support and the point at which the driving mechanism is locked (usually the driving motor). The elastic distortion of the latter parts is non-linear at low loads and careful calibration is required to give a set of values of K that can be applied at successive values of stress during relaxation. The values of K applying in the present tests were of the order of $10\text{--}20 \cdot 10^{-6} \text{ bar}^{-1}$. The amount of strain for a stress drop of 100 bars was therefore around 0.2–0.1%. The relaxation tests thus give a stress versus strain-rate relationship for a relatively small total strain interval at a stage subsequent to attaining a steady flow stress at the initial strain rate.

For optical observations ultra-thin sections of 1–2 μm thickness were prepared since many of the features of interest were smaller than standard section thickness and they also showed up more clearly at low interference colours under crossed polarizers. The sections were polished on both sides with Linde "B" alumina of grit size 0.05 μm and a low viscosity synthetic resin (Epirez 8859) was used to mount the section on glass. The sections for transmission electron microscopy were thinned by ion-beam bombardment.

RHEOLOGICAL OBSERVATIONS

Using the temperature interval 600°–1050°C, the flow behaviour of Carrara marble at laboratory strain rates has been studied for a range in differential stress from 1500 bars down to less than 100 bars. Apart from a slight continuing strain hardening at the lower temperatures, the flow stress closely approaches a constant or steady state value after a few percent strain in the constant strain rate experiments (Fig. 1). The steady state values of the flow stress are given in Table I and plotted logarithmically against strain rate in Fig. 2.

It is not possible to fit one simple empirical flow law to all the results in

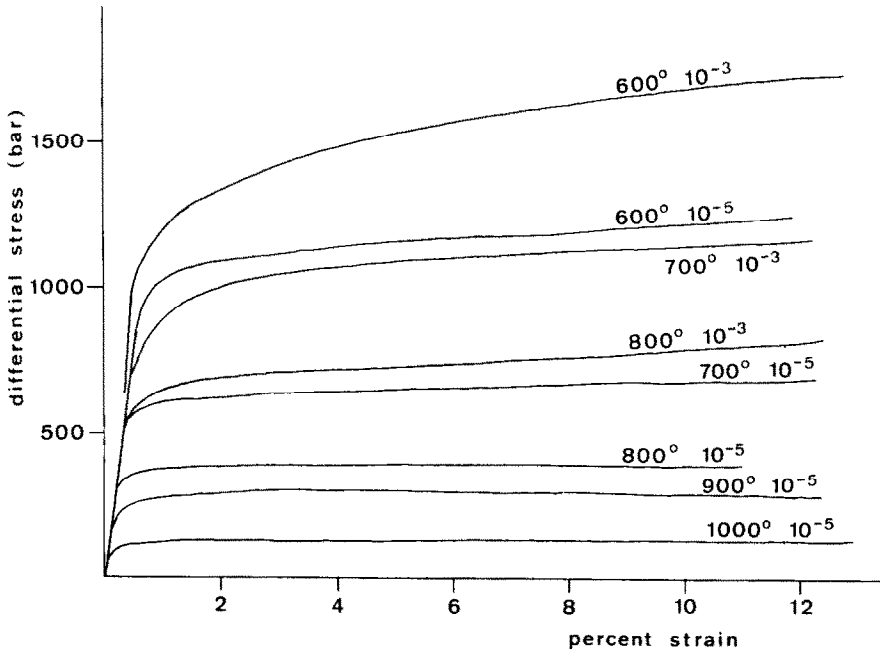


Fig. 1. Stress-strain curves for Carrara marble deformed under 3 kbar confirming pressure.

Fig. 2. The hyperbolic sine relationship between strain rate $\dot{\epsilon}$, temperature T and stress σ (Garofalo, 1965):

$$\dot{\epsilon} = A \exp(-H/RT) [\sinh(\sigma/\sigma_0)]^n$$

with four adjustable parameters A , H , σ_0 and n (H is the apparent activation energy for creep; A , σ_0 , and n are constants; R is the gas constant), could be fitted to all the observations above 200 bars but it would not at the same time fit those below 200 bars. We have preferred to fit commonly used three-parameter empirical relationships within more limited ranges of conditions. Therefore, starting with this aim, and drawing endorsement from relaxation and microstructural observations to be described later, we distinguish three deformation regimes defined by flow stress bounds as follows:

Regime 1 (>1000 bars). The exponential relationship:

$$\dot{\epsilon} = A \exp(-H/RT) \exp(\sigma/\sigma_0)$$

found by Rutter (1974) to apply up to 500°C with $A = 5.9 \cdot 10^5 \text{ sec}^{-1}$, $\sigma_0 = 114$ bars and $H = 62 \text{ kcal mole}^{-1}$, also fits our results at 600° and, for faster strain rates, at 700°C, with the same parameters. However, this fit does not extend below 1000 bars.

TABLE I

List of experiments (differential stress given at 10% shortening)

Run number	Temp. (°C)	Strain rate	Differential stress
4128	600	$1.0 \cdot 10^{-3}$	1695
2743 R	600	$1.0 \cdot 10^{-4}$	1435
2742	600	$1.0 \cdot 10^{-5}$	1219
2751 R	700	$1.0 \cdot 10^{-5}$	1148
2758 R	700	$1.0 \cdot 10^{-4}$	1031
2872	700	$1.0 \cdot 10^{-5}$	684
2736	800	$6.3 \cdot 10^{-3}$	929
2663 R	800	$1.0 \cdot 10^{-3}$	779
2695 R	800	$1.1 \cdot 10^{-4}$	593
2868	800	$1.1 \cdot 10^{-5}$	399
2698 R	900	$6.1 \cdot 10^{-3}$	626
2682 R	900	$1.0 \cdot 10^{-3}$	412
2692 R	900	$1.0 \cdot 10^{-4}$	355
2761 R	900	$2.1 \cdot 10^{-5}$	272
2685	900	$1.0 \cdot 10^{-5}$	296
2759	900	$5.3 \cdot 10^{-6}$	237
2761 *	900	$1.0 \cdot 10^{-6}$	153 (11%)
2853	1000	$6.7 \cdot 10^{-3}$	295
2850 R	1000	$1.0 \cdot 10^{-3}$	286
2704	1000	$1.1 \cdot 10^{-4}$	269
2849	1000	$1.1 \cdot 10^{-4}$	165
2836 *	1000	$1.1 \cdot 10^{-4}$	182 (10%)
2836 *	1000	$4.2 \cdot 10^{-5}$	146 (5.6%)
2836 *	1000	$4.2 \cdot 10^{-5}$	156 (13.3%)
2838 R	1000	$3.1 \cdot 10^{-5}$	140
2836 *	1000	$2.1 \cdot 10^{-5}$	136 (13.9%)
2837	1000	$1.1 \cdot 10^{-5}$	114
2837 *	1000	$1.1 \cdot 10^{-5}$	120 (16.6%)
2836 * R	1000	$1.1 \cdot 10^{-5}$	122 (15.3%)
2905	1000	$1.1 \cdot 10^{-5}$	151
2913	1000	$1.1 \cdot 10^{-5}$	124
2910	1000	$1.0 \cdot 10^{-5}$	132
2732	1000	$5.7 \cdot 10^{-6}$	94
2846	1000	$5.5 \cdot 10^{-6}$	95
2837 *	1000	$2.4 \cdot 10^{-6}$	77 (11.3%)
2920	1050	$1.0 \cdot 10^{-4}$	130
2920 * R	1050	$9.4 \cdot 10^{-5}$	142 (14.8%)
2840 R	1050	$3.1 \cdot 10^{-5}$	95
2916 * R	1050	$3.0 \cdot 10^{-5}$	101 (11.7%)
2916	1050	$1.1 \cdot 10^{-5}$	80
2920 *	1050	$1.0 \cdot 10^{-5}$	89 (12.4%)
2920 *	1050	$2.9 \cdot 10^{-6}$	70 (11.2%)
2916 *	1050	$1.1 \cdot 10^{-6}$	43 (11.0%)

* Variable strain rate tests, strain at which the strength was determined is given in brackets.

R = stress relaxation tests at end of test.

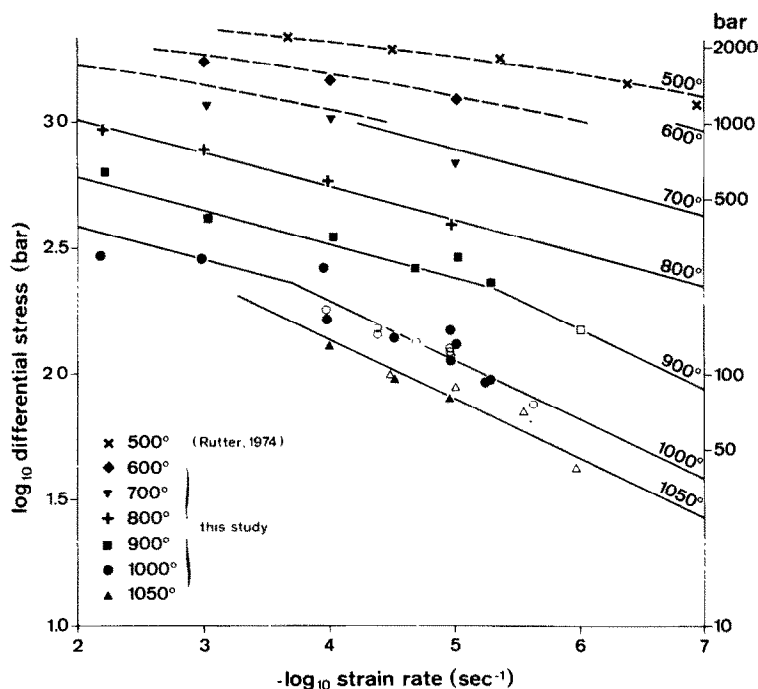


Fig. 2. Log-log plot of the differential stress vs. the strain rate of all constant and variable strain rate tests listed in Table I. Closed symbols: constant strain rate tests; open symbols: variable strain rate tests. Lines of best fit correspond to the parameters listed for regimes 2 and 3 in Table II (solid lines) and for flow regime 1 (broken lines, best fit after Rutter, 1974, as listed in Table II).

Regime 2 (200–1000 bars). In this regime, encompassing mainly the results at 800° and 900°C but extending to the lower strain rates at 700°C and the higher strain rates at 1000°C, the data best fit the power law:

$$\dot{\epsilon} = A \exp(-H/RT) \sigma^n$$

with $\log A = -4.5 \pm 0.4$ in sec/bar units, $H = 100 \pm 10$ kcal mole⁻¹ and $n = 7.6 \pm 0.8$ (these parameters were obtained from a least squares fit in the logarithmic plot for the data in the interval $200 < \sigma < 1000$ bars, minimizing the strain rate residual and quoting the first standard deviation). This fit cannot be satisfactorily extended to higher or lower stresses.

Regime 3 (<200 bars). Here the flow stress is clearly more sensitive to strain rate than in the other regimes. The narrower range and higher scatter of the data make it difficult to draw unequivocal conclusions about the flow law from the constant strain rate data alone. However, if data from strain rate stepping experiments are included (also shown in Fig. 2), and a power

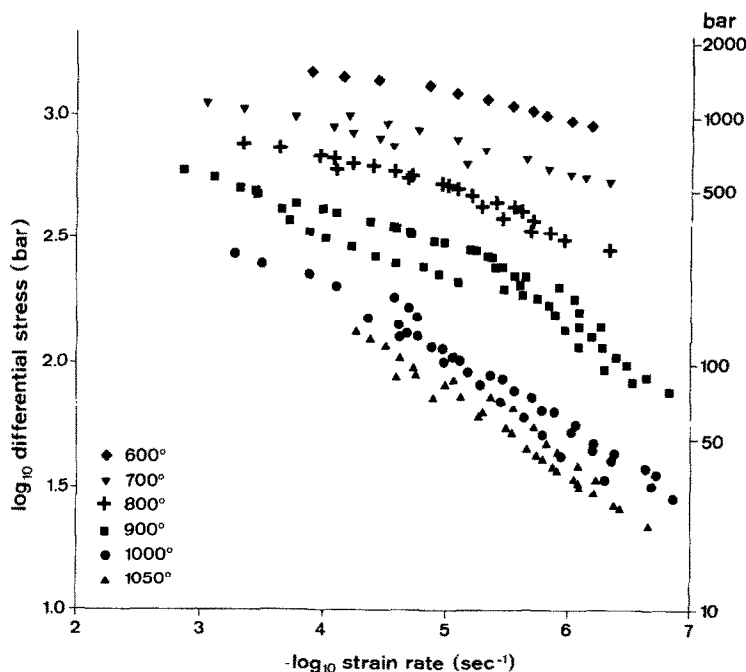


Fig. 3. Log—log plot of the differential stress vs. the strain rate for all the relaxation data (one experiment at 600°C, two experiments at 700°C, 800°C and 1050°C, three experiments at 900°C and 1000°C).

law is fitted in the same way to the combined data below 200 bars, the parameters characterizing flow in this regime are $\log A = 3.9 \pm 0.2$ in sec/bar units, $H = 102 \pm 11$ kcal mole⁻¹ and $n = 4.2 \pm 0.4$. Thus the apparent activation energy is indistinguishable from that in regime 2 but the stress exponent n appears to be roughly one half that in regime 2.

A marked decrease in n below 200 bars is also clearly indicated by relaxation tests (Fig. 3). Earlier experiments (Schmid, 1976) showed that in Solnhofen limestone the flow stress during relaxation is, to a first approximation, the same at a given strain rate as in a constant strain rate experiment and this appears also to hold for Carrara marble. Even if the small strains involved in the relaxation test are insufficient to ensure that a steady state flow stress is attained throughout relaxation, the relaxation stresses would probably reflect any change in mechanism below 200 bars that would give rise to a change in the steady state flow law. The relaxation results actually suggest that n may be even smaller than indicated by the fit in Fig. 2, possibly about $n = 3$, but with about the same apparent activation energy.

MICROSTRUCTURE

*Optical microscopy**Starting material*

The block of marble used is unfoliated and the grains show no initial shape anisotropy or crystallographic preferred orientation. The grain-size distribution is unimodal and the average grain size around 200 μm . The grains show no effects of previous deformation (Fig. 4); any deformation features have evidently been annealed out during regional metamorphism because this marble was certainly deformed in its geological setting (Camignani et al., 1978). The few very thin *e*-twin lamellae present are in random orientations and often terminate inside grains with no lattice distortion at their ends (compare deformation twins in Fig. 6). The grain boundaries are sutured but there are no signs of subgrain formation or recrystallization in the grain boundary area.

Specimens deformed in regime 1 (<1000 bars)

Observations in thin section reveal a preponderance of twinning in this regime (Fig. 5). The twins produced during the deformation are markedly

TABLE II
Comparative rheological behaviour in calcite rocks

	Solnhofen limestone	
Grain size (μm)	4	
Study by	Rutter (1974)	Schmid et al. (1977)
Temperatures ($^{\circ}\text{C}$)	up to 500	600–900
Confining pressure (kbar)	1.5	3
Flow law in regime 1 ($\dot{\epsilon} = $) *	$10^{-0.12} \exp\left(-\frac{47}{RT} + \frac{\sigma}{160}\right)$	consistent with Rutter
Stress at transition to regime 2 (bars)	—	1900
Flow law in regime 2 ($\dot{\epsilon} = $) *	—	$10^{-1.33} \exp\left(-\frac{71}{RT}\right) \sigma^{4.7}$
Stress at transition to regime 3 (bars)	—	1000 (600°)–400 (900°)
Flow law in regime 3 ($\dot{\epsilon} = $) *	—	$10^{2.7} \exp\left(-\frac{51}{RT}\right) \sigma^{1.7}$

TABLE II. Continued.

Carrara marble		
Grain size (μm)	200	
Study by	Rutter (1974)	this work
Temperatures ($^{\circ}\text{C}$)	up to 500	600–1050
Confining pressure (kbar)	1.5	3
Flow law in regime 1 ($\dot{\epsilon} =$) *	$10^{5.8} \exp\left(-\frac{62}{RT} + \frac{\sigma}{114}\right)$	consistent with Rutter
Stress at transition to regime 2 (bars)	—	1000
Flow law in regime 2 ($\dot{\epsilon} =$) *	—	$10^{-4.5} \exp\left(-\frac{100}{RT}\right) \sigma^{7.6}$
Stress at transition to regime 3 (bars)	—	200
Flow law in regime 3 ($\dot{\epsilon} =$) *	—	$10^{3.9} \exp\left(-\frac{102}{RT}\right) \sigma^{4.2}$
Yule marble		
Grain size (μm)	300–400	
Study by	Heard (1963); Heard and Raleigh (1972)	
Temperatures ($^{\circ}\text{C}$)	up to 800	
Confining pressure (kbar)	5 (extension tests)	
	1-orientation **	T-orientation
Flow law in regime 1 ($\dot{\epsilon} =$) *	$10^{7.8} \exp\left(-\frac{62}{RT} + \frac{\sigma}{91}\right)$	$10^{7.0} \exp\left(-\frac{57}{RT} + \frac{\sigma}{138}\right)$
Stress at transition to regime 2 (bars)	1100	1400
Flow law in regime 2 ($\dot{\epsilon} =$) *	$10^{-12.2} \exp\left(-\frac{62}{RT}\right) \sigma^{8.3}$	$10^{-11.3} \exp\left(-\frac{61}{RT}\right) \sigma^{7.7}$
Stress at transition to regime 3 (bars)	—	—
Flow law in regime 3 ($\dot{\epsilon} =$) *	—	—

* Units of sec, bar, kcal mole $^{-1}$, $^{\circ}\text{K}$; $\dot{\epsilon}$ = strain rate, R = gas constant, σ = differential stress, T = absolute temperature; the exponential fits for regime 1 in Yule marble are taken from Rutter (1974); the flow law in regime 1 refers to the stress at 10% strain in all cases.

** The 1-orientation is more favourable to twinning in extension than is the T-orientation.

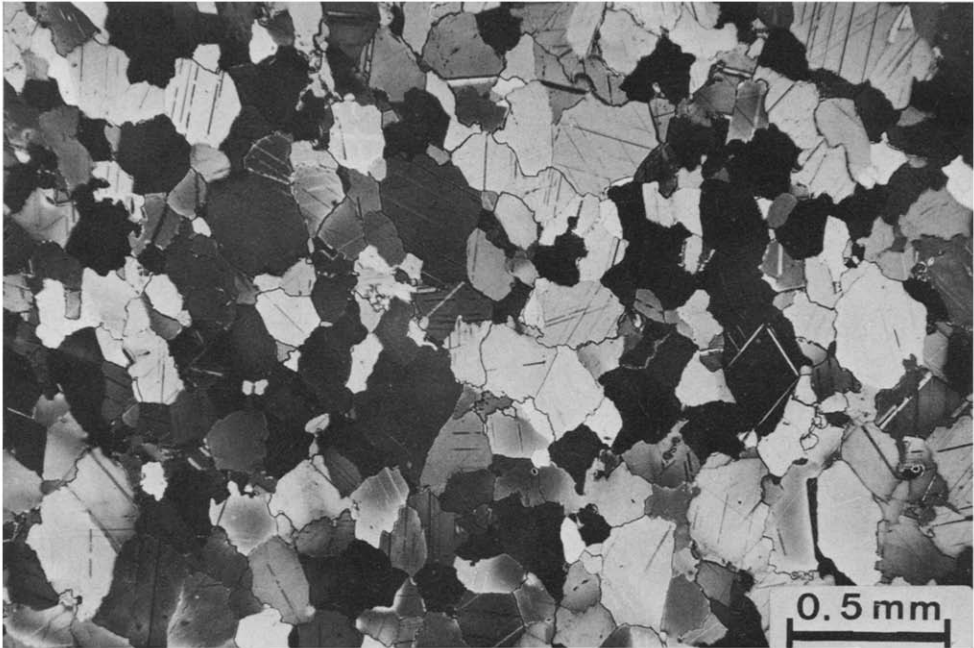


Fig. 4. Undeformed Carrara marble.

lensoid in shape, with constricted ends at grain boundaries or at intersection with other twins. This morphology makes them easily distinguishable from the narrow twin lamellae initially present or produced during cooling and depressurizing at the end of the experiment (Fig. 6) and it also allows distinction between the twinned and parent domains within a grain.

The width of the twinned domains varies from a few microns up to around $40\ \mu\text{m}$. Often more than half the grain is twinned on a single set, the *c*-axes of the twinned domains in such cases being invariably within 30° of the compression axis (U-stage measurement on 30 grains). Thus twinning is a powerful mechanism for re-orienting the *c*-axes subparallel to the compression axis, and this effect may be accentuated by external rotation (for example, the central part of the largest grain in Fig. 5). In grains with host *c*-axis orientation perpendicular to the compression axis, conjugate sets of *e*-twins develop (Fig. 6).

Strain compatibility requirements dictated by the shape and intersection of the twins, as well as by inhomogeneous external rotation (Fig. 5), require a considerable amount of slip dislocation movement as well as twinning in the grains. Evidence for this activity is seen, for example, in the undulatory extinction near twin intersections, and in grains with *c*-axis near the compression axis which remain untwinned (Figs. 5 and 6). The extent of these effects, including the tendency for broadening of a few twins in preference

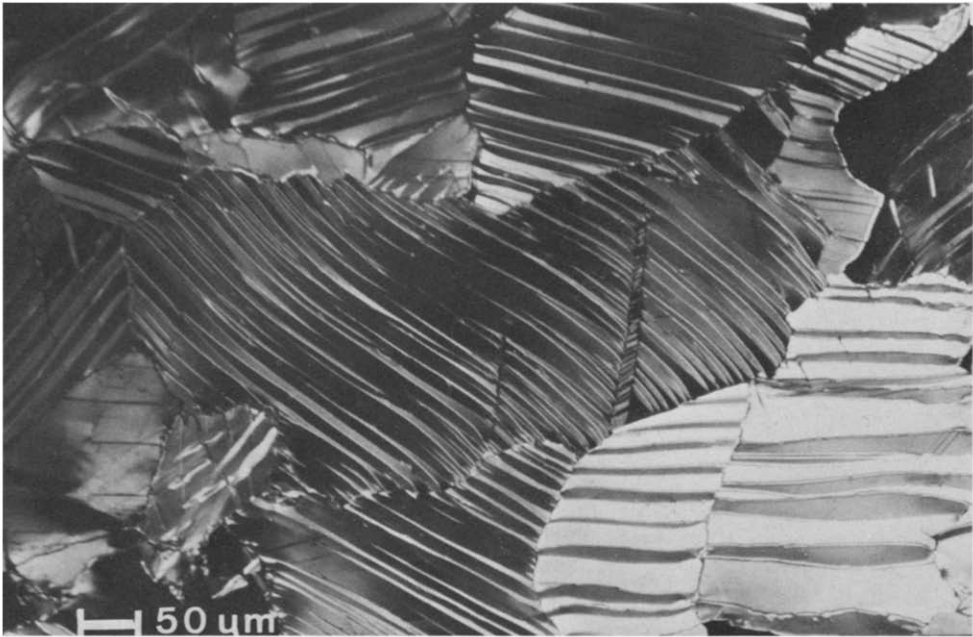


Fig. 5. Run 2871 (regime 1, 20% strain): in the central portion of the big grain twinning producing dextral shear went almost to completion (twinned domain in dark). The resolved shear stress coefficient on this e -plane, subperpendicular to the plane of the section, was determined to be 0.49 in the grain boundary area. The central portion is externally rotated by 15° in a sinistral sense around an a -axis sub-perpendicular to the plane of the section. Note also undulatory extinction in weakly twinned grains. The compression direction is vertical in Figs. 5–15.

to proliferation of many narrow twins, indicates that the ease of slip approaches that of twinning in regime 1. The onset of such a change in twin character has been observed near 300°C in 1-cylinders of Yule marble (Heard, 1963) and between 400 and 500°C in Carrara marble (Rutter, 1970). The upper boundary to regime 1 then, in turn, represents the completion of the transition from dominant twinning to deformation mainly by slip. This effect is illustrated in Fig. 8 in a specimen deformed near the boundary, where only small portions of the grain are seen to be twinned and the terminations of the twinned domains are marked by wedge-shaped deformation bands indicative of slip.

The formation of sub-grains and recrystallized grains is seen in this regime but is localized in grain boundary regions (Fig. 7); it will be discussed later. However, away from the grain boundaries, there are no signs of recrystallization within the grains like that in Yule marble which was observed to peak, along with the grain-boundary recrystallization, at 600°C (Griggs et al., 1960; note that the final strains and local strain rates were higher in their experiments than in ours).

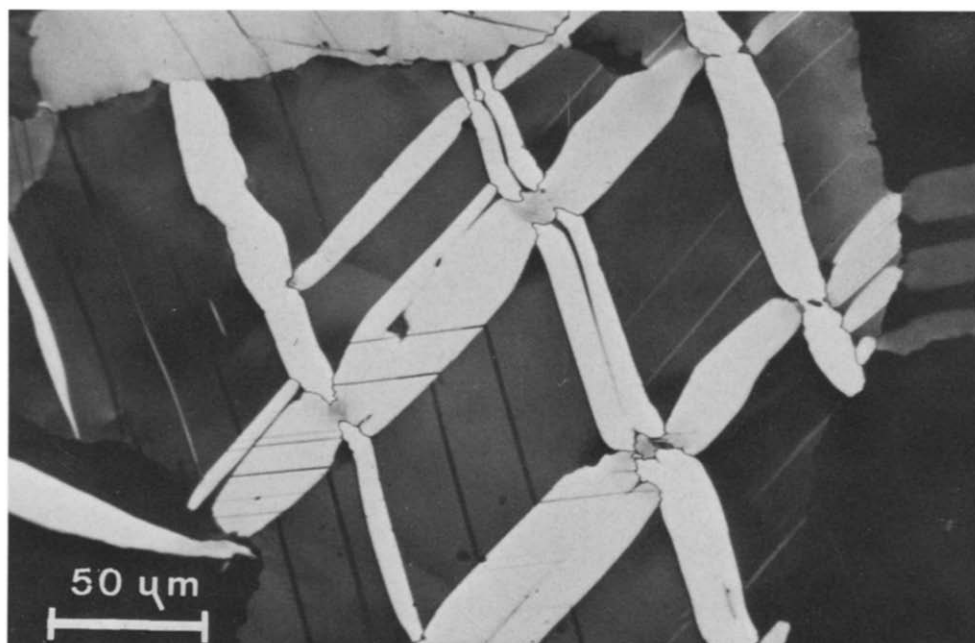


Fig. 6. Run 2743 (regime 1, 16% strain): conjugate twins with Schmid-factors of 0.40 (NE-trending set) and 0.20, respectively. Note mutual offset of twinned domains and also undulatory extinction with serrate twin boundaries at the nodes. Three twinned domains nucleate twins in the neighbouring grain at the right hand side of the micrograph. Undulatory extinction in the host domain. Note the presence of thin ϵ -lamellae within the twinned domains, probably induced by cooling and unloading after the deformation experiment.

Specimens deformed in regime 2 (200–100 bars)

This regime is characterized by the absence or paucity of twinning, by a strong but variable subgrain development within the grains and a distinctly different structural development near the grain boundaries (giving a “core and mantle” grain structure, Fig. 9), and by a high grain boundary mobility. In the main parts or cores of the grains away from the grain boundaries, there are all stages between general undulatory extinction, deformation bands defined by banded extinction, and irregularly shaped but generally elongate subgrains (Fig. 10). These subgrains are highly variable in dimensions in a given specimen, and their size does not appear to be correlated with the stress level.

The grain boundary or mantle regions exhibit a substructure consisting of an equi-axed mosaic of boundaries (Fig. 11). Across some of these boundaries the difference in orientation is small so that the enclosed domains can be classed as equi-axed subgrains. Across others the difference in orientation is sufficiently large that the domains can be classed as “recrystallized grains”, of the same size as the subgrains. Both subgrains and recrystallized grains are

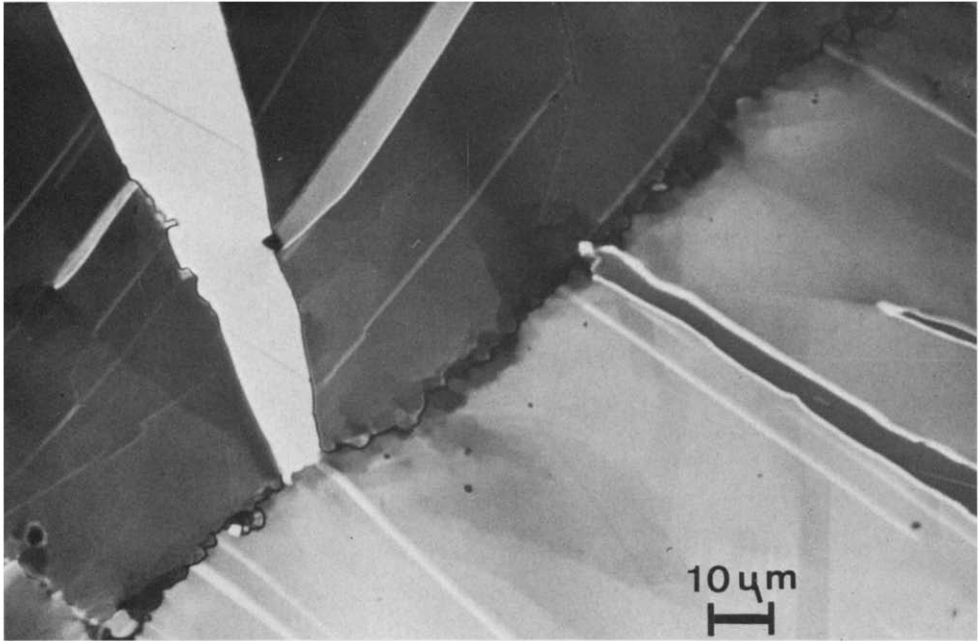


Fig. 7. Run 2742 (regime 1, 17% strain): equi-axed subgrains and recrystallized grains in the grain boundary region. Undulatory extinction and deformation bands in the grain interior. Note the locally serrate twin boundary of the twinned domain in the upper left side, suggesting mobility of twin boundaries.

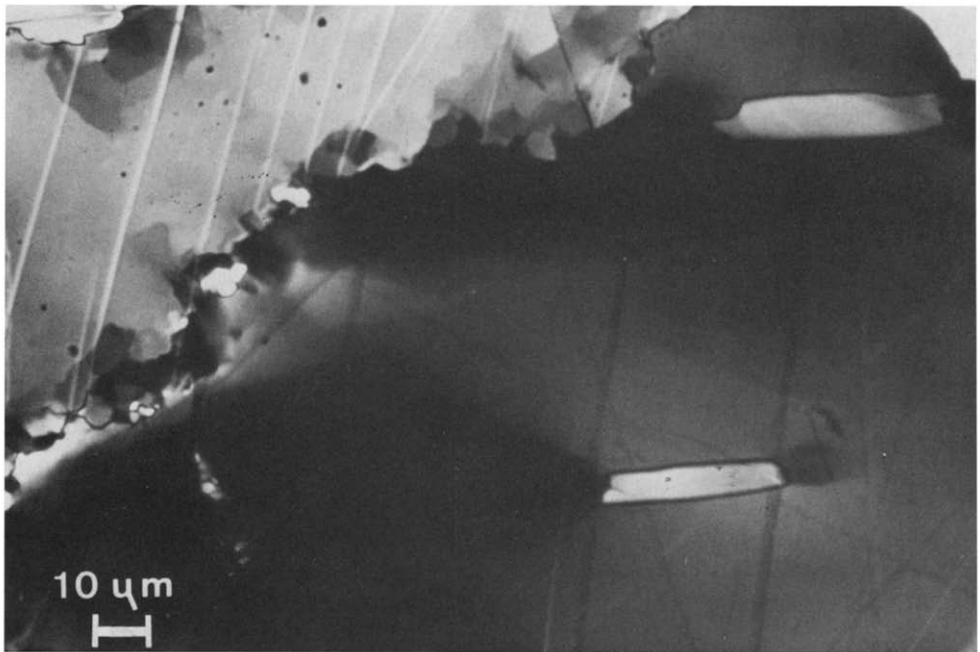


Fig. 8. Run 2758 (Boundary between regime 1 and 2, 12% strain): twinned domains terminating within the grain and "strain shadows" at the points of termination. Formation of subgrains and primary recrystallization in grain boundary area.



Fig. 9. Run 2685 (regime 2, 30% strain): core mantle structure with undulose extinction. Deformation bands and irregularly shaped subgrains in the core, equi-axed subgrains and primary recrystallized grains in the grain boundary region.

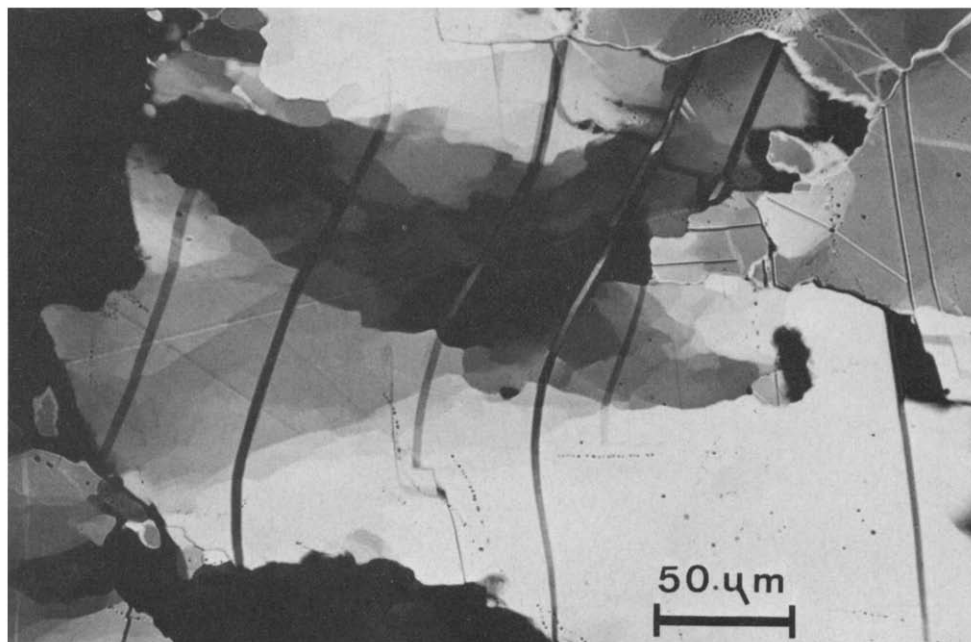


Fig. 10. Run 2685 (regime 2, 30% strain): deformation band subdivided into subgrains; the shear produced is indicated by the internal rotation of preexisting *e*-lamellae, now in an irrational orientation in respect to the host *c*-axis.

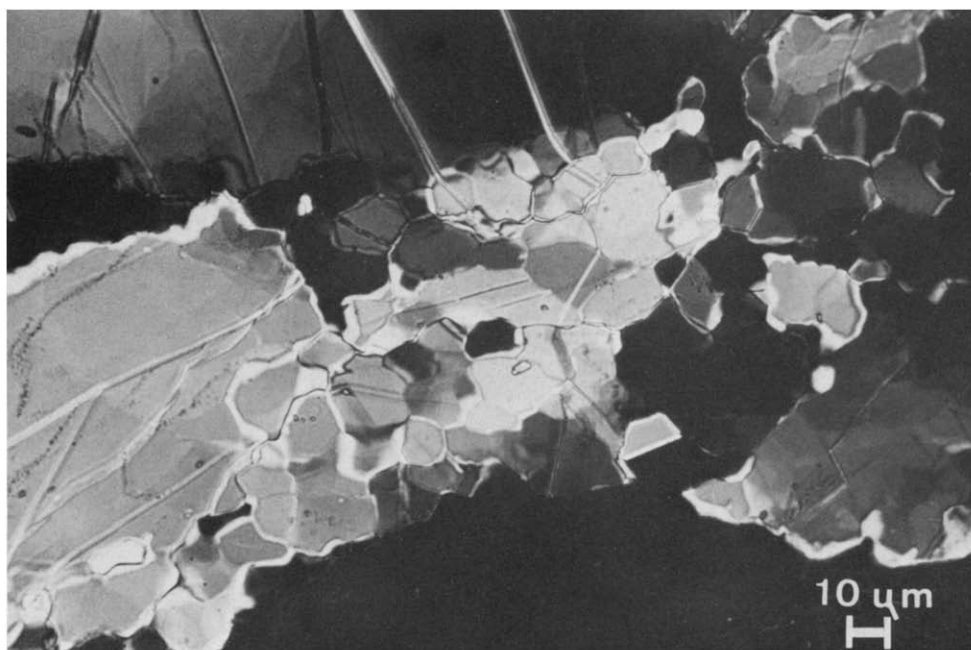


Fig. 11. Run 2685 (regime 2, 30% strain): equi-axed subgrains and primary recrystallization in a grain boundary area.

of a fairly constant size that can be related to the flow stress, as discussed later.

The original grain boundaries develop a highly convoluted or scalloped shape (Fig. 12). The appearance in cross-section of groups of insular domains of identical optical orientation in close proximity points to an intricate spatial interpenetration of neighbouring grains as a result of a high grain boundary mobility, although at this stage there is no tendency for particular grains to enlarge grossly at the expense of others. Viewed at low magnification, however, the grain boundaries appear to align along two conjugate directions bisected by the compression direction; the significance of this alignment is not clear.

Specimens deformed in regime 3 (<200 bars)

On entering this region, the equi-axed substructure that mantled the grains in regime 2 begins to fill entire grains (Fig. 13) suppressing the core and mantle structure characteristic of regime 2. Now the original grains become wholly subdivided by a recrystallization that overprints the original microstructure at high strains (Fig. 15) and shows the correlation between grain size and flow stress discussed later.

At 1000° and 1050°C, this microstructure is further overprinted in part

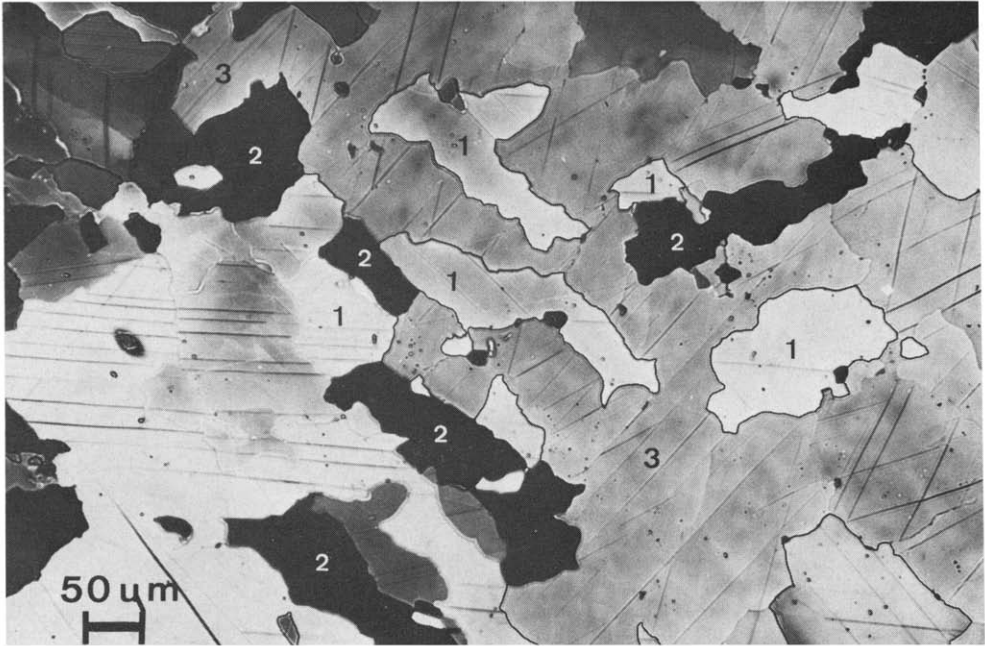


Fig. 12. Run 2868 (regime 2, 17% strain): insular domains with identical optical orientations, suggesting high grain boundary mobility. Domains labelled with the same number belong to the same grain.

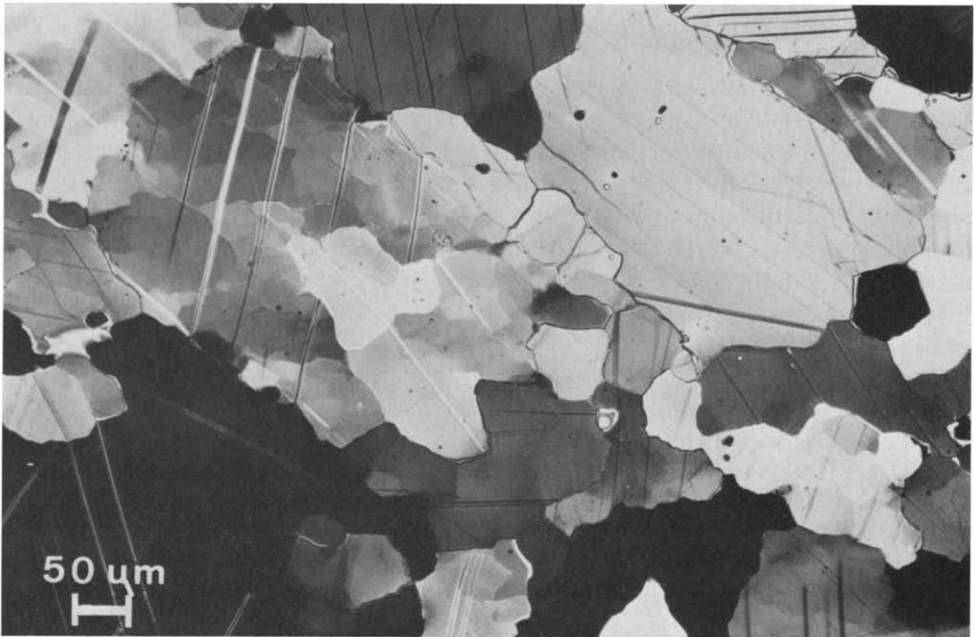


Fig. 13. Run 2905 (regime 3, 21% strain): equi-axed subgrains and recrystallized grains penetrate the entire domain of old grains.

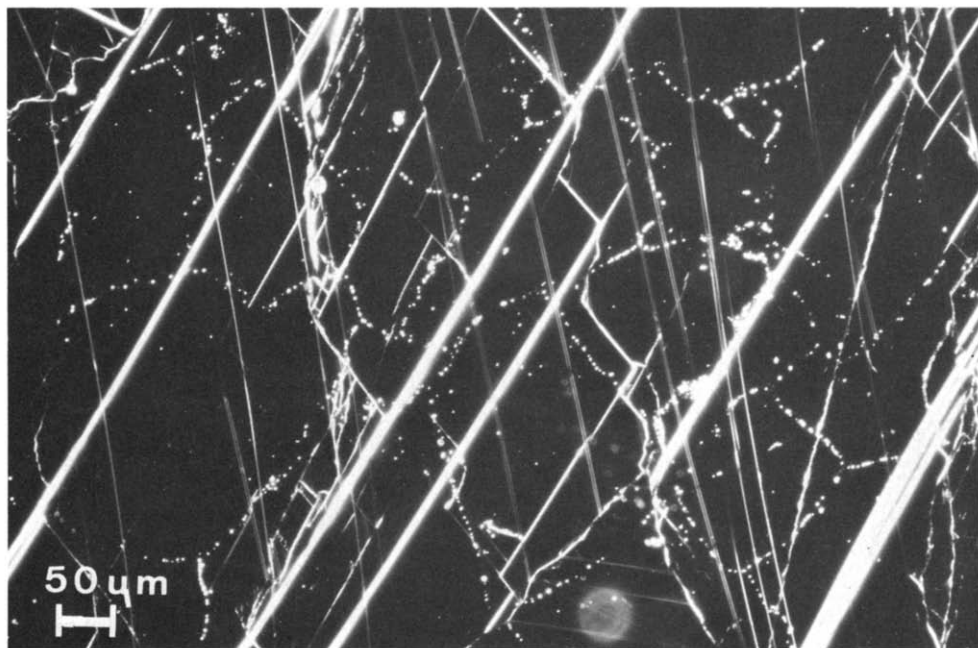


Fig. 14. Run 2846 (regime 3, 2% strain): "dark field" micrograph obtained under illumination subparallel to the plane of the section. The entire domain of the micrograph is occupied by a single crystal (note the contrast produced by continuous *e*-lamellae) which is the product of secondary recrystallization. Old grain boundaries are marked by the alignment of CO₂ bubbles. These inclusions are the product of some calcite decomposition occurring at the beginning of the experiment until the equilibrium CO₂ pressure is reached. The *e*-lamellae are slightly bent indicating syntectonic grain growth.

by an exaggerated grain growth or secondary recrystallization in which certain grains grow to more than 1 mm (Fig. 14). The boundaries of these enlarged grains have a similarly convoluted shape to that noted for the original grains in regime 2 (cf. Fig. 12). The enlarged grains occur grouped in substantial areas within the specimens but with no tendency to appear preferentially in regimes of higher or lower strain such as in the centre or near the ends. Some of them are practically free of strain features but others are re-deformed and it is therefore concluded that they grow during deformation. The *c*-axis orientations of 62 such grains, measured from several specimens and combined in one diagram, showed only a very weak tendency to align at a high angle to the compression direction.

The change in microstructure with increasing strain in regions relatively unaffected by the exaggerated grain growth is shown in Fig. 15. There is a clear tendency for the average grain size to approach the size of the equiaxed recrystallized grains as larger strains are approached. Thus grainsize reduction through recrystallization rather than flattening of original grains dominates the microstructural development with increasing strain. It is nota-

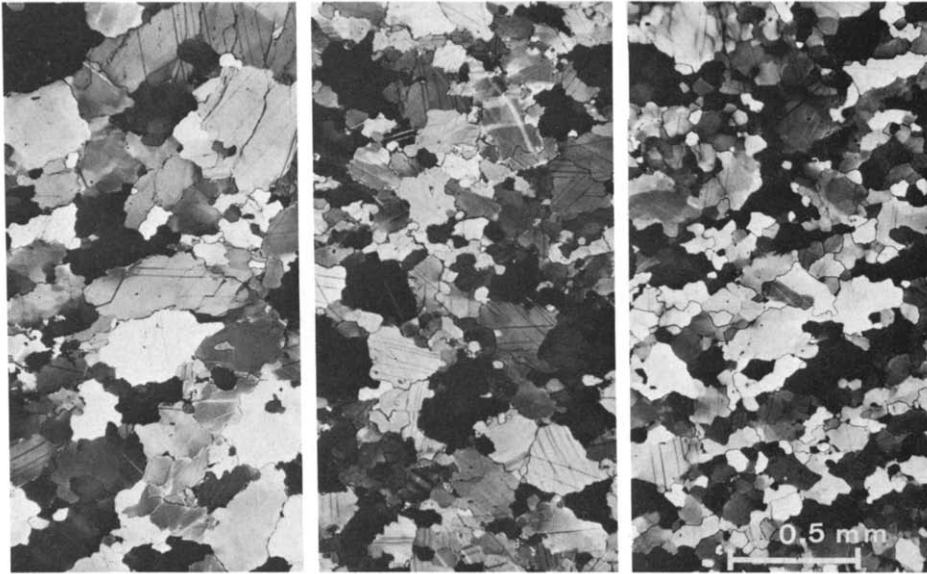


Fig. 15. Run 2913, 2905 and 2910 (deformed under identical conditions within regime 3 up to 11, 21 and 32% shortening, respectively, increasing strain from left to right hand side): Note that the grain size reduction with increasing strain is the dominant microstructural change in areas of the sections relatively unaffected by secondary recrystallization.

ble that this progression continues over a large range in strain, well beyond the stage at which a steady-state flow stress is attained.

Grain boundary displacements

Additional experiments were carried out to measure the displacements at grain boundaries. Following the technique described by Schmid et al. (1977), prepolished split cylinders were deformed and the polished surfaces (separated during deformation either by a copper or gold foil) were examined by both optical microscope and scanning electron microscopy. Relative grain boundary displacements were observed by the topographical relief at the boundaries. The vertical step-heights, \bar{v}_r , at the boundaries were measured on the optical microscope using the fine-focus vernier. The average displacement, \bar{v}_r , for each specimen was determined from at least 100 measurements along a longitudinal traverse. The strain due to grain boundary sliding was calculated, using $e_{\text{gbs}} = \phi \bar{v}_r / d$, where d is the average grain size and ϕ the geometrical factor relating the vertical displacement at the grain boundary to the shortening strain — ϕ is taken to be 1.4 following the observations and discussion by Bell and Langdon (1969) and Gifkins (1973). The results are given in Table III.

No grain boundary sliding occurs at 600°C, in the exponential flow

TABLE III
Grain boundary displacements

Run	Temp ($^{\circ}\text{C}$)	$\dot{\epsilon}$ (sec^{-1})	e_T (%)	e_{gbs}/e_T ^a (%)	\bar{u}_r ^b (μm)	% contrib. ^c
4211	600	10^{-4}	15	~ 0	0	0
4217	800	10^{-4}	19	14	2.6	71
4278	1000	10^{-3}	15	12	1.7	61
4223	1000	10^{-4}	15	25	3.3	74
4276	1000	10^{-5}	8	38 (48) ^d	2.95	82
4281	1000	10^{-6}	~ 1.5	59 (66) ^d	1.05	55

^a e_{gbs}/e_T %: the percentage of the total strain due to the grain boundary sliding.

^b \bar{u}_r : the mean offset at grain boundaries.

^c % contrib: the percentage of grain boundaries contributing the measured offset.

^d Measurement restricted to the central portion of the specimen.

regime. At 800°C and at the higher strain rates at 1000°C , in the "high- n power law flow regime", some grain boundary sliding is observed but its contribution to the overall strain is minor. However, at lower strain rates at 1000°C , where n is lower, this contribution becomes more significant, amounting to roughly half the overall strain. The grain boundary offsets occur at the boundaries of both original and recrystallized grains and sliding can be presumed to occur at most grain boundaries since roughly two-thirds or more of the grain boundaries intersected by the split show a component of displacement normal to it (Table III) and in many of the others there may be a displacement approximately parallel to the polished face (no pre-existing scratches remain after the experiment to check this point). Although the average offsets are between 1 and $3\ \mu\text{m}$, there are some values as high as $15\ \mu\text{m}$.

The topographic relief on the pre-polished surfaces is complex. Figures 16a and b illustrate the non-uniformity of the grain boundary sliding (Fig. 16b also includes an example of sliding of a recrystallized grain). Also illustrated is a rumpling (marked *W*) near several triple-joint junctions. This effect may be partly imprinted from the copper foil but similar effects have been observed in deformed Solnhofen limestone at 900°C using gold foil. The rumpling therefore probably indicates that accommodation of the sliding occurs at least in part by inhomogeneous deformation within the grains. Occasional slip steps or twin lamellae were observed (marked *S*) but these may be formed during cooling.

Electron microscopy

Starting material

The grains are initially divided into subgrains, of minimum size about

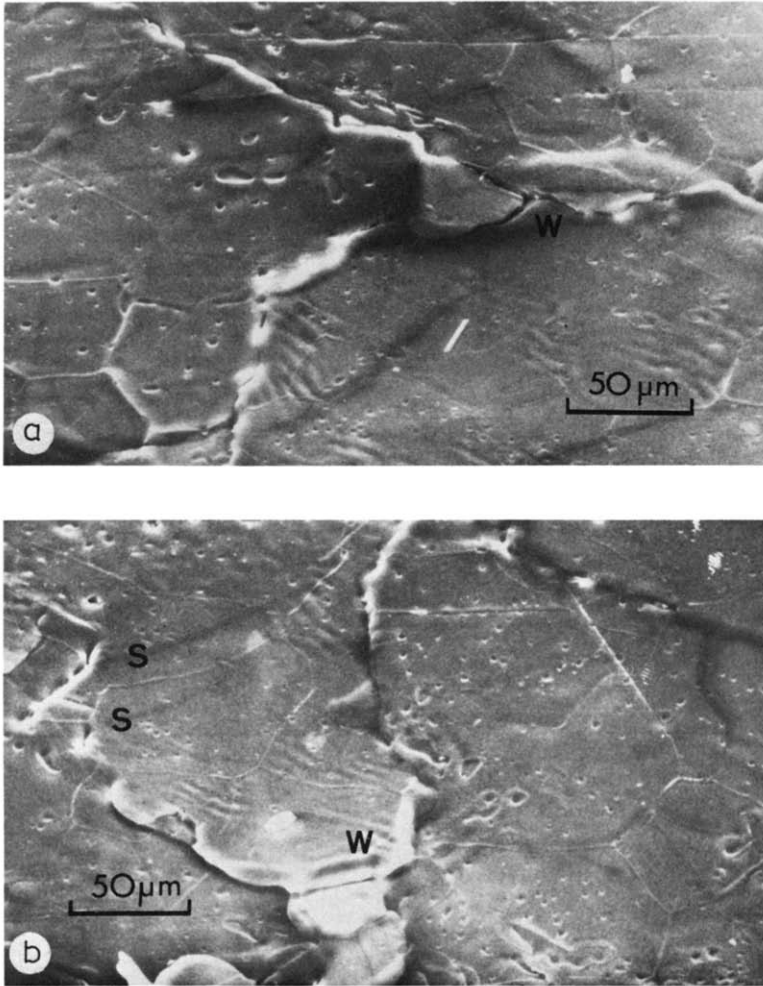


Fig. 16. Scanning electron micrographs of the surface of split cylinders after deformation. For explanation see text.

3 μm , by low angle sub-boundaries composed of dislocation networks such as shown in Fig. 17a. Within the subgrains there are “free” dislocations of various configurations, including: (a) curved segments; (b) isolated interactive networks; and (c) small loops aligned parallel to larger dislocation segments and commonly associated with kinks in the dislocations (Fig. 17b); the latter configuration is suggestive of trailing loops (Hull, 1975). The initial density of the free dislocations is relatively high and is variable, ranging from $1 \cdot 10^8$ to $1.3 \cdot 10^9 \text{ cm}^{-2}$.

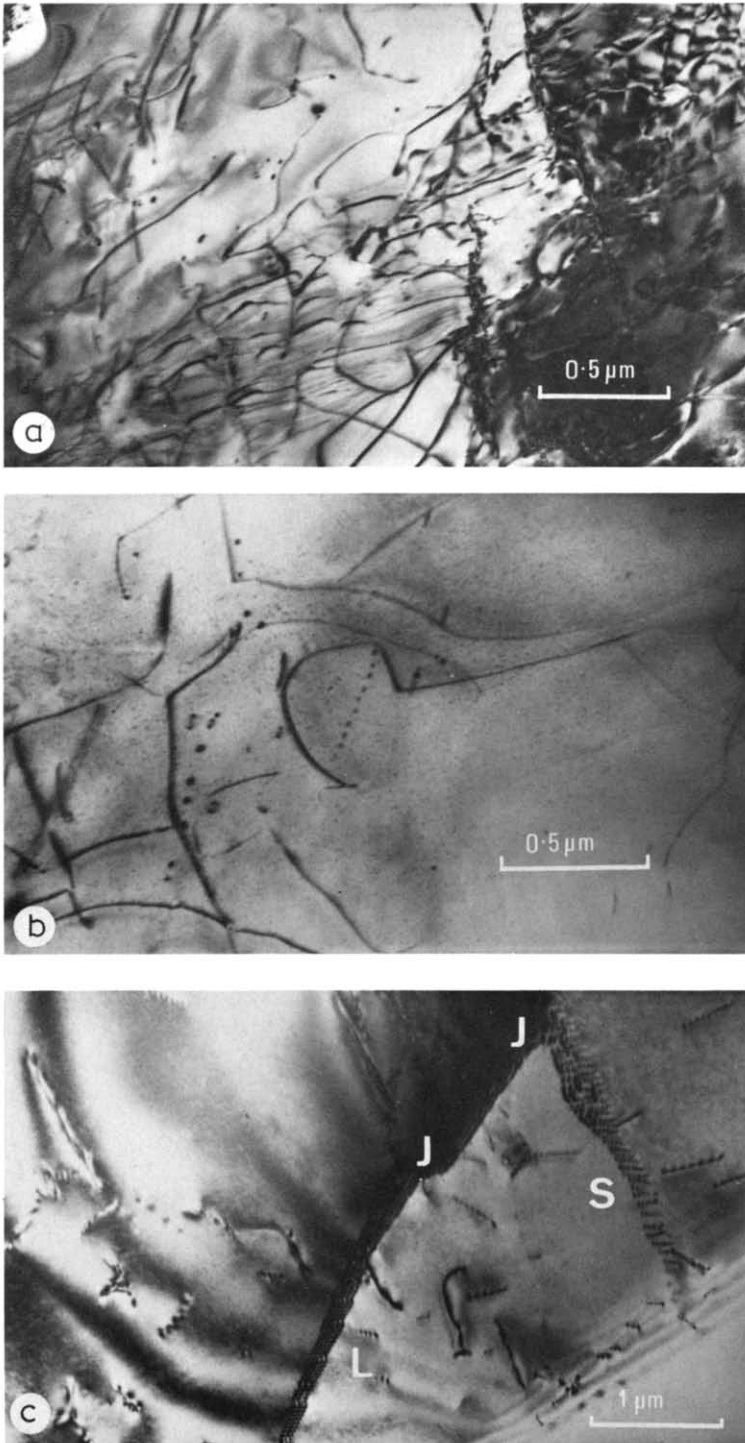


Fig. 17. Transmission electron micrographs. For explanation see text.

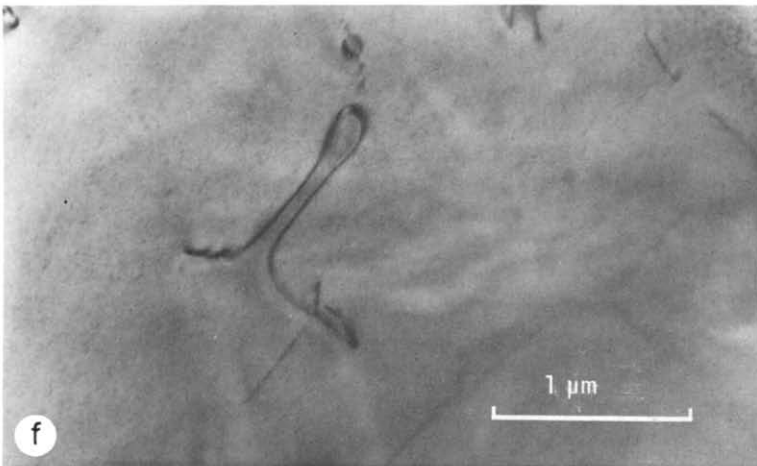
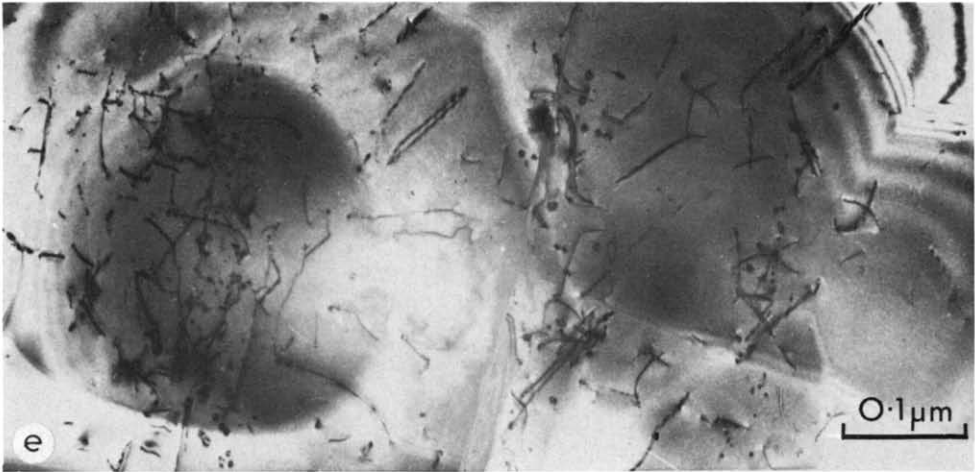
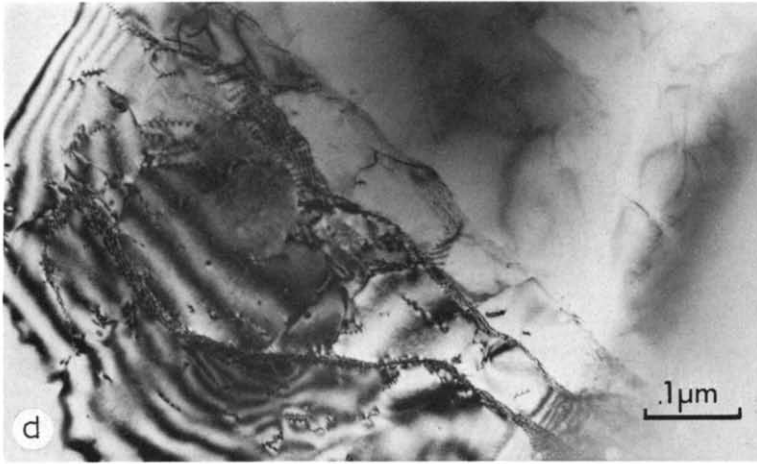


Fig. 17. e-f. For legend see p. 265.

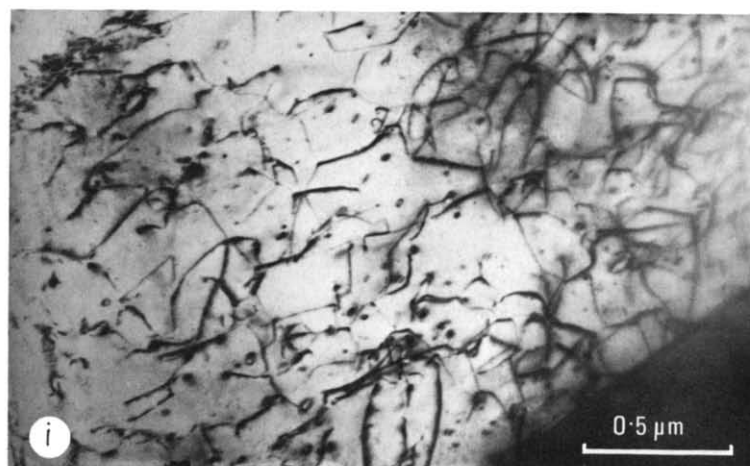
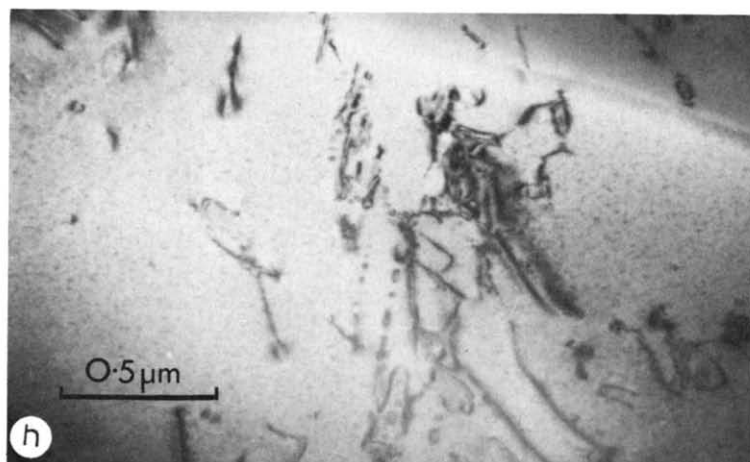
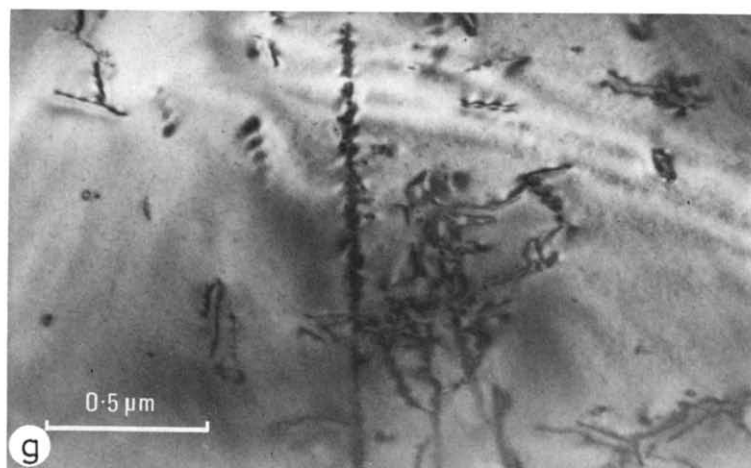


Fig. 17. g-i. For legend see p. 265.

Specimens after deformation

The deformed specimens have low angle sub-boundaries of the type shown in Fig. 17c. These show prominent ledges, marked *L*, and the dislocations may be arrayed into simple tilt configurations, as at *S*, or into more complex networks, involving sub-boundaries forming junctions, as at *J*. In specimens deformed in the high-*n* regime (for example, 2663, as shown in Fig. 17d), the substructure is predominately elongate. The subgrain size is markedly variable within a given specimen.

In specimens deformed in the high temperature, low stress field, the free dislocations within the subgrains are distributed rather non-uniformly (Fig. 17e). From observations on the planes in which the dislocations now lie, it would appear that $r(10\bar{1}4)$ (and/or $e(01\bar{1}8)$), $f(01\bar{1}2)$ and $a(11\bar{2}0)$ slip planes have all been active (the Miller-Bravais indices are referred to the structural unit cell). Dipole configurations are frequently observed, as well as high densities of loops, within the regions of high dislocation density. The loops appear to form by a pinching-off process as shown in Fig. 17f. In addition to the fluctuations in density shown in Fig. 17e, extremely localized dislocation concentration is also commonly observed. An example is shown in Figs. 17g, h. This is a feature that appears linear when viewed edge-on (Fig. 17g), with a width commensurate with the normal image width of a dislocation; however, on tilting, the projected image reveals a complex array of dislocation segments and loops (Fig. 17h). The array is parallel to $r(01\bar{1}4)$, an often-reported slip plane, and the image contrast behaviour is consistent with the Burgers vector being $\langle 2021 \rangle$. However, the array may not represent a single slip plane but a few active slip planes very closely spaced. The dislocations in this array have interacted to produce loops, dipoles and interactive nodal points.

In specimens deformed at lower temperatures and higher flow stresses, the dislocations are more uniformly distributed within the subgrains (Fig. 17i). There are fewer small loops, but the number of interactive nodal points or junctions is greater.

The mean dislocation densities have been determined by counting the dislocations intersected in a number of linear traverses, and averaging the counts to give the values plotted in Fig. 18; the bars indicate the variances among the traverses, which are especially large at low stresses because of the non-uniform distribution noted earlier. Only the results above 600 bars could be fitted by the commonly-observed relationship $\sigma \propto \rho^{1/2}$, where σ is the stress and ρ the dislocation density. The results at the lower stresses conform more nearly to a $\sigma \propto \rho^3$ relationship; that is, here the dislocation density would appear to be unexpectedly high and unusually insensitive to the level of the flow stress.

At first sight, noting that the dislocation densities giving the latter unusual trend fall within the range of initial densities, it could be questioned whether sluggish kinetics had prevented equilibration to a lower density (Goetze and Kohlstedt, 1977). However, annealing experiments indicate that this is not

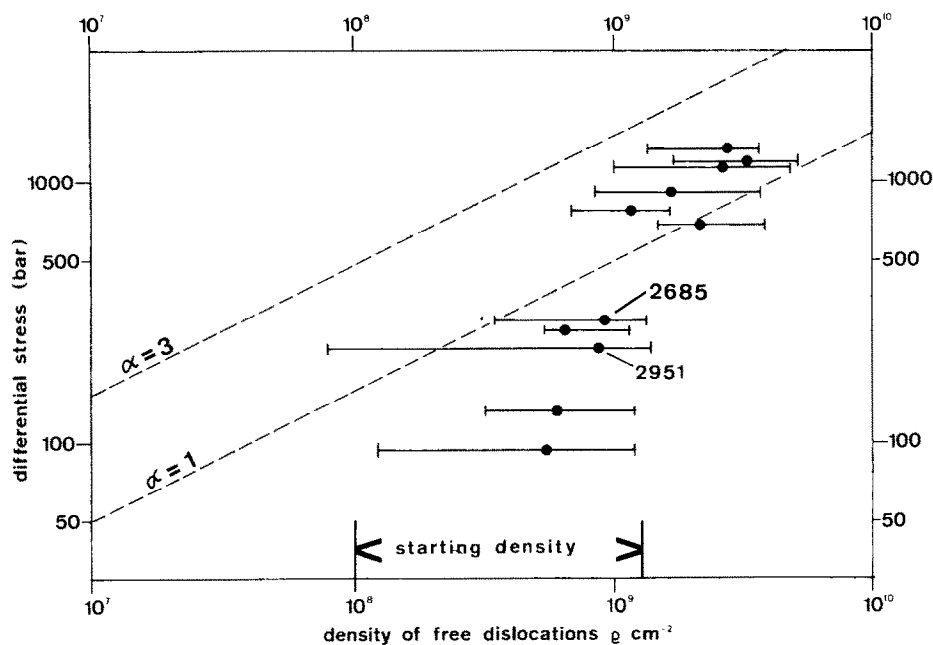


Fig. 18. Log-log plot of the dislocation density vs. the differential stress. Lines for values 1 and 3 of constant α in a relationship $\sigma = \alpha \mu b \rho^{1/2}$ are superimposed for the purpose of comparison with observations ($\mu = 0.25$ mbar, $b = 6.3$ Å).

so. Thus annealing unjacketed Carrara marble under CO_2 at 50 bars pressure for 2.5 hours at 925°C reduced the dislocation density by an order of magnitude. On the other hand, specimen 2685 amongst the group in question above had remained at 900°C for 8.5 hours during its deformation, a time that should have been adequate for re-equilibration on the basis of the annealing experiment, and the situation is even more favourable for re-equilibration at 1000°C .

The effects of dislocation recovery on the mechanical strength were demonstrated in an experiment in which a specimen was annealed under 3 kb pressure at 900°C for 1 hour. The temperature was dropped to 800°C and the deformation testing commenced immediately. Compared with specimens deformed under identical conditions without this prior annealing, this specimen had a distinctly lower initial yield stress and the work-hardening stage of the stress-strain curve, prior to steady-state flow, was more extensive (Fig. 19). This behaviour was readily reproducible and it demonstrates the rapid rearrangement of dislocations into lower energy configurations given sufficient thermal activation during the high temperature annealing.

Hence, the explanation of the unexpectedly high dislocation densities at low stresses appears to lie in the strains induced in the grains during cooling under pressure after the deformation. These strains arise from the anisotropy

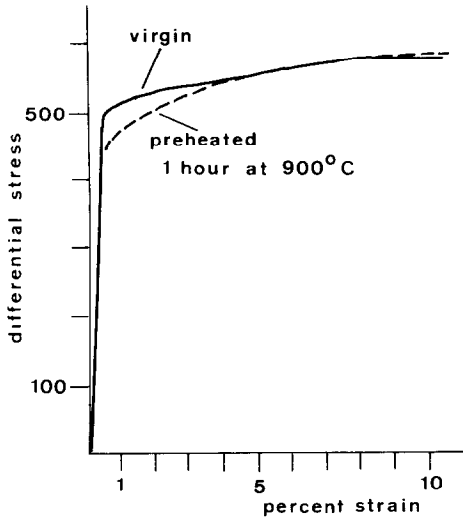


Fig. 19. Tests at 800°C, 10^{-4} sec $^{-1}$ strain rate, 3 kbar confining pressure.

of thermal contraction, which would be expected to give a potential misfit between grains, equivalent to strains of the order of one percent (Paterson, 1963). In heating or cooling an unjacketed specimen, as in the annealing experiment just described, the grain boundaries part and the differential contraction is expressed mainly in opening up gaps at grain boundaries. Such opening-up is prevented in jacketed specimens under pressure and so the grains are strained plastically at the lower temperatures during the cooling. Dislocation features such as shown in Figs. 17g, h may have arisen in this way at a relatively low temperature and in general the cooling under pressure can be expected to contribute substantially to the average dislocation density. In the case of the unjacketed specimens heated and cooled in CO₂ at 50 bars, the grain boundaries were observed to be parted and the fewer dislocations present were mainly concentrated in grain-boundary regions, especially near crack-tips (cf., case of olivine: Boland and Hobbs, 1973).

Finally, the question of possible dislocation rearrangements arises in high pressure experiments since there is a short interval of about a minute between releasing the load and commencing the cooling process. Such post-deformation recovery was checked on specimen 2951 that was cooled under the differential stress reached during steady state flow. This stress was maintained to immobilize the dislocations active during the high temperature deformation, but it was not sufficient to activate dislocations during the cooling process. Although specimen 2951 showed an unusual range in its dislocation density, the average density is comparable with similarly deformed specimens cooled without the differential stress being applied. If any dislocation recovery had occurred, its effects are completely overprinted by the amount of deformation induced during the cooling as discussed earlier.

Relation of grain size to flow stress

The current interest in grain size—stress relationships (for example, Twiss, 1977) has prompted a corresponding examination of the Carrara marble specimens. This has revealed a good correlation with flow stress in the case of the equi-axed recrystallized grains and the corresponding optical-scale subgrains, and a possible correlation for the minimum size of the electron microscope EM-scale subgrains (Fig. 20).

It follows from the previous descriptions that three categories of grains can be distinguished: (1) original grains, highly strained; (2) grains with highly convoluted grain boundaries, including those showing exaggerated grain growth; (3) equi-axed new grains on the scale of the equi-axed substructure that begins to dominate the microstructure in regime 3. It is not difficult to select objectively the grains in the last category and to determine their average diameter, as measured in the thin section. This was done for 50 grains per specimen and the average grain sizes are shown in Fig. 20, together

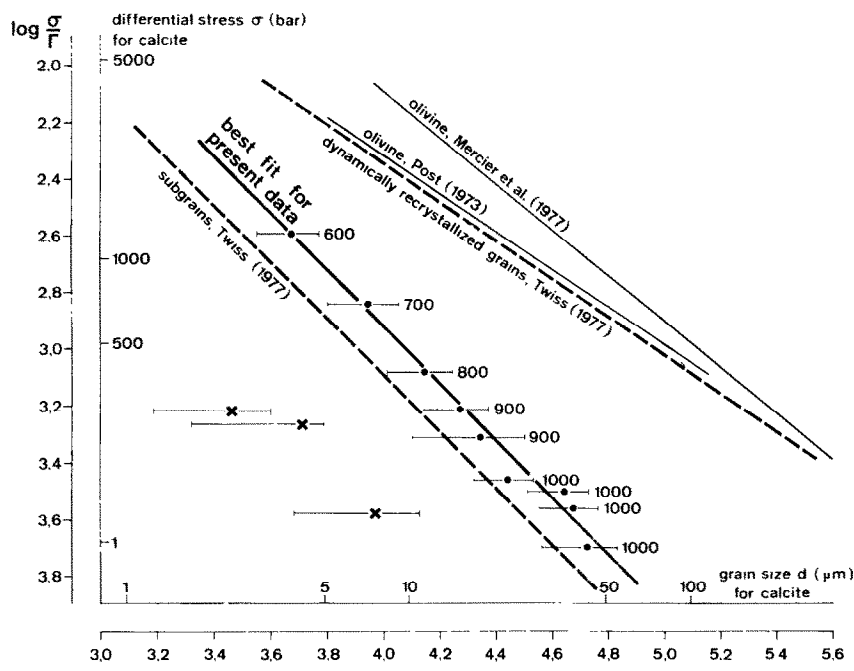


Fig. 20. Normalized log—log plot of the optically determined grain size produced during dynamic in situ recrystallization as a function of differential stress (points). For each experiment the variance of the individual measurements and the test temperature in °C are given. Subgrains on the EM-scale (crosses) are plotted for comparison. Stress and grain size are normalized with those values for the elastic constant Γ and the Burgers vector b given by Twiss (1977) for marble. For discussion see text.

with the variances of the individual measurements. In specimen 2910 (1000°C , $10^{-5} \dot{\epsilon}$), in which 50 recrystallized grains of $>10^{\circ}$ orientation difference gave a measured grain size of $38 \pm 9 \mu\text{m}$, 50 subgrains were also measured, giving a size of $37 \pm 10 \mu\text{m}$. Thus, the sizes of both subgrains and "recrystallized" grains can be taken as being identical. The sizes in Fig. 20 were all obtained from recrystallized grains since they are easier to measure. The slope of the logarithmic plot against flow stress is 1.01 ± 0.05 , showing that within the stress range from 100 to 1000 bars the grain size of the equiaxed recrystallized grains, and of the corresponding subgrains, is almost exactly inversely proportional to the flow stress and varies from 43 to $5 \mu\text{m}$, respectively.

The EM-scale subgrains are less easy to analyse on account of the wide variability in their size and shape. However, if the smallest subgrains are selected and their mean size is plotted against flow stress in the same logarithmic plot (Fig. 20), they define very roughly a line of similar slope to that given by the optical scale subgrains and recrystallized grains but displaced nearly an order of magnitude towards smaller sizes.

ANALYSIS AND DISCUSSION

Relation to previous work

A comparison of the present observations with results from other studies on several calcite rocks is given in Table II and Fig. 21. It is seen that, while the fine-grained Solnhofen limestone is stronger than the coarser-grained marbles up to about 500 or 600°C (roughly half the absolute melting point), the marbles are stronger at higher temperatures, the difference reaching an order of magnitude at 900°C . The relative weakening of Solnhofen limestone at the higher temperatures is related to the strong development of grain boundary sliding in its "superplastic" regime, a regime not reached in the marbles because of their coarser grain size (Schmid, 1976; Schmid et al., 1977). It is also notable that, in spite of only small difference in grain size, there is a substantial difference in strength between the two marbles themselves, much greater than the difference between the two orientations of the anisotropic Yule marble (it seems unlikely that this difference arises from the use of extension in the latter, especially since the mean stress is roughly one-third higher; no obvious pressure effects appear between our results and Rutter's in Carrara marble at 500 – 600°).

In general, twinning only contributes significantly to the deformation in *regime 1* and here it appears to contribute to the lower strain-rate sensitivity of the flow stress, that is, to a higher dependence of the strain rate on the stress. This effect is seen by comparing the flow laws for the T -orientation of Yule marble (less favourable to twinning than the 1 -orientation) and for Solnhofen limestone (where relatively little twinning was observed) with the other examples in Table II. Greater twinning activity also appears to lower

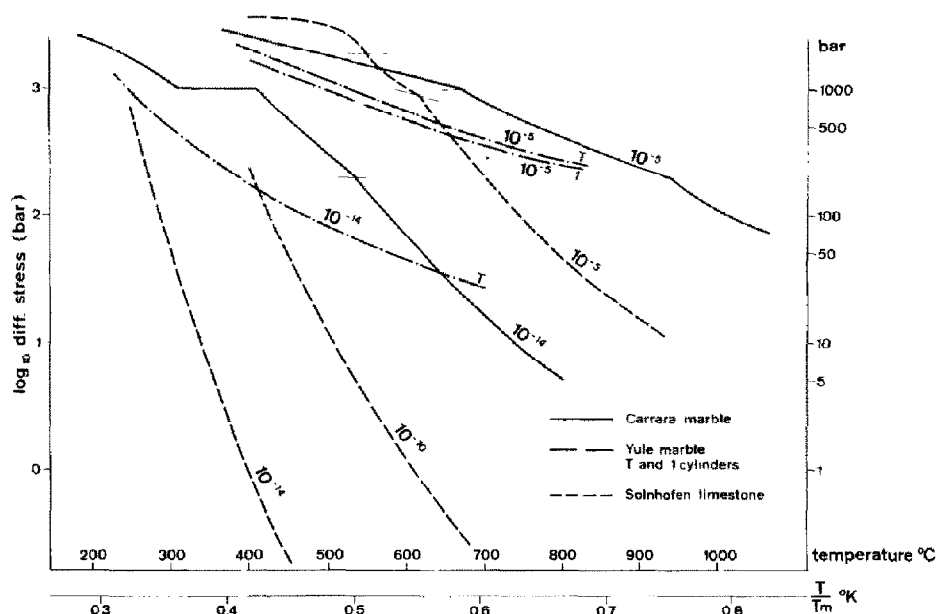


Fig. 21. Plot of the logarithm of the differential stress vs. the temperature analogous to a deformation mechanism map. For Carrara marble the flow laws obtained from constant strain rate tests as listed in Table II were used, for Yule marble the best fits of Heard and Raleigh (1972) were used as listed in Table II and for Solnhofen limestone the data of Schmid et al. (1977) were used. Boundaries between different flow laws are shown by horizontal lines. The strain rate contours are given in sec^{-1} .

the transition stress to regime 2. These two effects thus indicate that twinning is an important factor in determining the exact form of the flow law in regime 1 and that its suppression is a precondition for entering the power law regime 2 (consistent with the microscopical observations in the present study). On the other hand, the values of the apparent activation energy H in regime 1 are less clearly correlated with the degree of twinning.

There are two particularly interesting aspects of the behaviour in *regime 2* where power law creep enters. First, there are the unusually high values of the stress exponent n in the marbles, Carrara in this respect being the same as Yule; in Solnhofen limestone n is lower, raising the question of whether Solnhofen in this regime is already affected by a small contribution from the grain boundary sliding that becomes predominant in regime 3. Second, the apparent activation energies H are markedly different in the two marbles; while for Yule marble the value of H is about the same as in regime 1, that in Carrara marble is markedly higher. For Solnhofen limestone, H is also higher in regime 2 than in regime 1 but in both regimes the flow is less temperature sensitive than for Carrara marble. The value of $100 \text{ kcal mole}^{-1}$ for H for steady state flow in regime 2 in Carrara marble appears to be slightly above that for self-diffusion of carbon and oxygen in calcite ($88 \text{ kcal mole}^{-1}$,

Anderson, 1969; however, if only the flow data for 800° and 900°C in the middle of regime 2 are considered, a value of about 90 kcal mole⁻¹ is obtained for flow, equal within experimental uncertainty to that for self-diffusion).

The transition below 200 bars to a *regime 3* of flow in the Carrara marble is a new observation for marble. Although some grain boundary sliding has been detected in this regime, it nevertheless appears distinctly different in characteristics from the "superplastic" regime 3 of Solnhofen limestone with its very low n and reduced H . The value of H for Carrara is the same in regime 3 as in regime 2, within experimental uncertainty, but n has fallen to near 4, a value similar to that for Solnhofen in regime 2. The question remains of (1) whether the latter observation indicates the absence of a factor responsible for unusually high n in marbles which is also absent in Solnhofen in regime 2, or (2) whether the small amount of grain boundary sliding noted in Carrara in regime 3 is reducing the value of n , or (3) whether there is some other explanation for the lower n in Carrara in regime 3.

A correlation between the steady flow stress σ and the size d of subgrains and recrystallized grains has not previously been demonstrated in marble. The present observations are consistent with the subgrain and grain sizes being solely a function of stress of the form $\sigma \propto d^{-p}$ although unfortunately a lack of overlap of grain size data at different temperatures prevents an unambiguous confirmation of this relationship to stress alone. Such a relationship is well known in metals and ionic materials (see, for example, McQueen and Jonas, 1975; Poirier, 1976) and has been reported for olivine and quartz rocks (Post, 1973, 1977; Kohlstedt et al., 1976; Mercier et al., 1977). The exponent p is usually found to have values in the range 0.7–1, with a tendency for subgrains to give 1 and recrystallized grains the lower values (McQueen and Jonas, 1975). Such relationships have been rationalized in terms of internal energy considerations and particular assumptions about the inter-relationships of dislocation density, boundary energy and flow stress (see Twiss, 1977, and other writers quoted by him). Thus, Twiss deduces the theoretical relations given in Fig. 20, from which it is seen that the observed size of both subgrains and equi-axed recrystallized grains in the marble is in agreement with Twiss's predictions for subgrains but not for "dynamically recrystallized grains". Since Twiss quotes many observations from the literature that are approximately consistent with his two predicted lines, this feature of the marble results suggests that the recrystallization in the marble occurs by a distinctly different mechanism from the production of dislocation-free new grains considered by Twiss, a conclusion that is consistent with the description earlier of the equi-axed new grains in the marble developing by progressive disorientation of subgrains while maintaining the same size.

Mechanisms of deformation and recrystallization

The new results reveal a greater complexity of deformational behaviour in calcite rocks than hitherto suspected but, at the same time, the emerging

pattern shows more features in common with certain metallic and ionic materials. These features presumably reflect the deformation processes and may be common to many non-silicate rocks.

The twinning which appears only in regime 1 does not seem to be the primary control on the rheological behaviour even in this regime, since the measured flow stresses are much higher and more temperature sensitive than the stresses known to be required for twinning of calcite crystals at these temperatures (Griggs et al., 1960; Turner and Heard, 1965). The actual stress level and the microscopical observations both point to the rate-controlling step in the flow being a slip dislocation process involved in achieving full strain compatibility between adjoining domains within the specimen (cf., Von Mises compatibility condition), either between grains or between a lensoid shaped twin domain and its surroundings. Evidently, when this rate-controlling dislocation process becomes sufficiently easy that the macroscopic flow stress falls below 1000 bars, the grains in twinning orientations can be deformed with less total work by relatively uniform dislocation slip on one or two of the highly stressed slip planes than by developing a twin domain of defined finite strain that must be accommodated by a rather complex pattern of strain in the surrounding areas; the latter strain would be achieved by inhomogeneous multiple slip involving, in many parts, dislocation movement on planes not favourably oriented for a high resolved shear stress component from the macroscopic applied stress. However, when twinning does occur it will profoundly affect the preferred orientation developed and in this way have some indirect influence on the rheology. Also, since the stress distribution between twin and host regions will be inhomogeneous, the actual form of the flow law will be determined in a complicated way through a combination of the properties of the twinning and slip processes.

There may also be an inhomogeneous stress distribution in regime 2, corresponding to the "core and mantle" grain structure and again making it difficult to give a simple interpretation of the flow law. However, in regime 3 the structure is fairly uniform within the grains, possibly in part due to the difficulties of accommodation between grains being reduced by a degree of grain-boundary sliding. Thus in regime 3 the observed flow law may directly reflect the flow process that is predominant in the mantles of the grains in regime 2 and in the whole grains in regime 3 and which is characterized structurally by the development of equi-axed subgrains and new grains whose size is correlated with the stress. This flow law, a power law with n around 4 and apparent activation energy equal to or slightly above that for self-diffusion, is of a type commonly interpreted in terms of models of recovery creep with the velocity of climb of dislocations as the rate-limiting step (Weertman, 1975; Poirier, 1976, chapter 7).

Such a view suggests that the flow law in regime 2 then represents a combination of power law creep with $n \sim 4$ in the grain mantle and a less strain-rate sensitive creep in the cores of the grains (possibly like the slip part of the creep in regime 1), giving a flow of intermediate strain-rate sensitivity

expressible as the power law with $n \sim 8$; however, the apparent activation energies present a difficulty in accepting this interpretation since the value in regime 2 is equal to that in regime 3 rather than intermediate between those in regimes 1 and 3. An alternative interpretation could be that the observed flow law with $n \sim 8$ in regime 2 is dominated by, and characteristic of, the flow in the mantles of the grains in regime 2 and of the whole grains in regime 3, and that the higher bulk strain-rate sensitivity in regime 3 reflects a contribution from the grain boundary sliding to the total strain rate, the latter having a very high strain-rate sensitivity (cf., regime 3 with $n = 1.6$ in Solnhofen limestone: Schmid et al., 1977). Much more detailed studies of the rheological properties characteristic of the different structural developments is needed to clarify these issues before more detailed interpretation of the flow laws in terms of models of the dislocation processes is attempted.

An interesting feature of the present observations is that an effectively steady flow stress is attained at relatively small strains while the optical microstructure continues to evolve even up to 30% strain. Evidently the structural aspects such as the size of the equi-axed subgrains and new grains that are correlated with the stress are consequential on rather than determinative of the basic flow mechanism that itself determines the flow law. Any structural parameters involved in the flow law may represent aspects of the microstructure more subtle or fundamental than those obvious under the optical microscope but which determine the ultimate development of the latter in a way analogous to the development of equiaxed new grains from subgrains.

The recrystallization to the new equi-axed grains apparently occurs by the mechanism of progressive misorientation of subgrains that was invoked by Hobbs (1968) to explain the dynamic recrystallization which he observed in experimentally deformed synthetic quartz single crystals and by Poirier and Nicolas (1975) to explain recrystallization observed in naturally-deformed olivine rocks. This type of recrystallization, called in-situ recrystallization by Poirier and Nicolas, is distinct from the nucleation and growth mechanism that commonly occurs in annealing after cold-working but that can also occur during hot-working in some metals. The behaviour of the Carrara marble suggests analogy with metals of high stacking fault energy. In a review of high temperature behaviour in metals, McQueen and Jonas (1975) correlate the "restoration" processes in metals with high and low stacking fault energy. Metals with low stacking fault energy tend not to develop cell or subgrain structures in the way that those with high stacking fault energy do; on the other hand, the former tend to recrystallize by nucleation and growth during large hot-work deformations whereas the latter adjust to hot-work by recovery processes. The dynamic balance in Carrara marble is evidently also maintained by recovery processes rather than by nucleation-and-growth recrystallization but the subgrains formed in the recovery can develop an in-situ recrystallization by further misorientation. The nucleation-and-growth recrystallization described in Yule marble by Griggs et al. (1960) is presum-

ably the eventual response to deformation in a higher stress regime (regime 1), but it may also reflect differences in impurities in solid solution in the calcite which also affect the strength as noted earlier.

Geological implications

For geological usage the laboratory data have to be extrapolated into realistic strain rates (10^{-10} – 10^{-14} sec $^{-1}$) and temperatures (most of the experiments were performed at temperatures much higher than the ones expected in the upper crust, where calcite rocks are abundant). The deformation maps produced by Ashby (1972) illustrate that there exist different fields in a plot of stress vs. temperature, each field being characterized by a distinct deformation mechanism and consequently a different flow law.

Figure 21 is somewhat similar to such a deformation mechanism map, but the constitutive equations used are based on experimental evidence alone. It is a composite graph for three different calcite rocks (compare Table II) and for clarity only a few strain rate contours are shown.

The major feature of Fig. 21 is the substantial difference in flow stress between superplastically deforming fine-grained limestone (Solnhofen limestone) and the coarser grained marbles. The contrast in extrapolated strength between Carrara marble and Solnhofen limestone can be as high as 1 : 1000 at 400°C and a strain rate of 10^{-14} sec $^{-1}$. Thus, big "competence contrasts" can be expected to arise in a calcareous rock suite with domains of varying grain size at elevated temperatures.

There are discrepancies in the rheology of the two marbles as well and they cannot be explained in terms of grain size. This shows that other factors apart from grain size and mineralogical composition influence the flow properties. These factors are not yet understood and therefore extrapolations based on experimentally derived flow laws of one rock type should be taken with reservation.

Another difficulty arises from the fact that regimes 1 and 2 for Carrara marble are characterized by substantially different activation energies. If one assumes the transition stress between the regimes to be temperature independent, as observed within the laboratory conditions, an offset of the extrapolated strain rate contour results at geological strain rates (10^{-14} sec $^{-1}$ contour in Fig. 21). This probably indicates that the empirical form of our flow laws is inadequate for exact extrapolations.

The paleostress may be estimated directly by using the size of subgrains or dynamically recrystallized grains (Fig. 20). This makes it possible to check on the extrapolations if temperature and strain rate can be estimated from other geological evidence. When using grain size for paleostress determinations care must be taken to ensure that (1) the grain size is not controlled by impurities or second phase minerals and (2) that, on the basis of microstructural observations, the mechanism of recrystallization is the same as the one described for the experimentally deformed material. The experiments also

show that even after strains of up to 30% shortening no unique equilibrium grain size predominates the microstructure but that the grains used for paleo-stress determinations have to be selected carefully.

At very large natural strains it is to be expected that large domains within a rock will completely recrystallize to a new stress-determined grain size. If this new grain size is sufficiently small to cause a change in mechanism into a grain size-sensitive mechanism such as grain boundary sliding or superplasticity then the rheological properties of a recrystallized domain will change drastically. Carrara marble for example is expected to flow at a strain rate of $10^{-15} \text{ sec}^{-1}$ at 400°C and 800 bars differential stress (extrapolating the flow law for regime 2, Table II). According to Fig. 20 this means that these domains will recrystallize to a grain size of around $5 \mu\text{m}$. This is the grain size of a rock like Solnhofen limestone which is expected to deform superplastically at this temperature and stress level (Schmid et al., 1977). If the flow law for superplastically deforming Solnhofen limestone is extrapolated to 400°C and 1000 bar then a strain rate of around 10^{-9} sec^{-1} results.

Thus, a very marked increase in strain rate at constant stress (or conversely a stress drop at constant strain rate) is expected even if one allows for substantial errors by extrapolating. This work softening effect induced by syntectonic recrystallization and a change in mechanism may play an important role in the formation of shear zones and mylonite layers. In such a situation, however, the size of the syntectonically recrystallized grains may only indicate the peak stress during the initial stages of the strain history when the rock deformed by dislocation creep. The final stress may have been much lower as a consequence of work softening induced by a change in deformation mechanism.

ACKNOWLEDGEMENTS

This work was undertaken while two of the authors held fellowships at the Research School of Earth Sciences at the Australian National University. Help and advice from members of the staff, particularly the technical assistance from Peter Percival and Paul Willis are gratefully acknowledged. We also thank Prame Chopra for providing the results given in Fig. 19. Amongst many colleagues we had the opportunity to discuss and exchange ideas with, we would like to particularly mention Chris Goetze (MIT) who made a major impact on our thinking through his and his groups work. The first manuscript was critically read by B. Chapple, A. Pfiffner, J.G. Ramsay and E.H. Rutter.

REFERENCES

- Anderson, T.F., 1969. Self diffusion of carbon and oxygen in calcite by isotope exchange with carbon dioxide. *J. Geophys. Res.*, 74: 3918–3931.
Ashby, M.F., 1972. A first report on deformation mechanism maps. *Acta Metall.*, 20: 887–897.

- Bell, R.L. and Langdon, T.G., 1969. In: R.C. Gifkins (Editor), *Interfaces Conference*. Butterworths, Sydney, pp. 115–137.
- Boland, J.N. and Hobbs, B.E., 1973. Microfracturing processes in experimentally deformed peridotite. *Int. J. Rock Mech. Min. Sci.*, 10: 623–626.
- Carmignani, L., Giglia, G. and Kligfield R., 1978. Structural evolution of the Apuane Alps: an example of continental margin deformation in the northern Apennines, Italy. *J. Geol.*, 86: 487–504.
- Garofalo, F., 1965. *Fundamentals of creep and creep-rupture in metals*. Macmillan Series in Material Science. Macmillan, New York, 258 pp.
- Gifkins, R.C., 1973. The measurement of grain-boundary sliding in polycrystalline specimens. *Met. Sci. J.*, 7: 15–19.
- Goetze, C. and Kohlstedt, D.L., 1977. The dislocation structure of experimentally deformed marble. *Contrib. Mineral. Petrol.*, 59: 293–306.
- Griggs, D.T., Turner, F.J. and Heard, H.C., 1960. Deformation of rocks at 500°C–800°C. *Geol. Soc. Am. Mem.*, 79: 39–104.
- Heard, H.C., 1963. Effects of large changes in strain rate in the experimental deformation of Yule marble. *J. Geol.*, 71: 162–195.
- Heard, H.C. and Raleigh, C.B., 1972. Steady-state flow in marble at 500–800°C. *Geol. Soc. Am. Bull.*, 83: 935–956.
- Hobbs, B.E., 1968. Recrystallization of single crystals of quartz. *Tectonophysics*, 6: 353–401.
- Hull, D., 1975. *Introduction to Dislocations*. Pergamon Press, Oxford, 2nd ed., 259 pp.
- Kohlstedt, D.L., Goetze, C. and Durham, W.B., 1976. Experimental deformation of single crystal olivine with application to flow in the mantle. In: S.K. Runcorn (Editor), *Petrophysics: The Physics and Chemistry of Minerals and Rocks*, Wiley, London, pp. 35–49.
- McQueen, H.J. and Jonas, J.J., 1975. Recovery and recrystallization during high temperature deformation. In: *Treatise on Materials Science and Technology*, Vol. 6, *Plastic Deformation of Materials*. Academic Press, New York, N.Y., pp. 393–493.
- Mercier, J.C., Anderson, D.A. and Carter, N.L., 1977. Stress in the lithosphere: Inferences from steady state flow of rocks. In: M. Wyss (Editor), *Stress in the Earth*. Reprint from *Pageoph.*, 115 in *CCRG*, 3: 199–226, Birkhäuser Verlag, Basel.
- Paterson, M.S., 1963. Secondary changes in length with pressure in experimentally deformed rocks. *Proc. R. Soc. London Ser. A*, 271: 57–87.
- Paterson, M.S., 1970. A high-pressure high-temperature apparatus for rock deformation. *Int. J. Rock Mech. Min. Sci.*, 7: 517–526.
- Paterson, M.S., 1977. Experience with an internally heated gas-medium deformation apparatus to 500 MPa. 2nd Int. Conf. on High Pressure Engineering, Brighton, 1975. The Institution of Mechanical Engineers.
- Poirier, J.P., 1976. *Plasticité à Haute Temperature des Solides Cristallins*. Eyrolles, Paris, 320 pp.
- Poirier, J.P. and Nicolas, A., 1975. Deformation-induced recrystallization by progressive misorientation of subgrain-boundaries, with special reference to mantle peridotites. *J. Geol.*, 83: 707–720.
- Post, R.L., 1973. *The Flow Laws of Mt. Burnet Dunite*. Thesis, Univ. of California, Los Angeles.
- Post, R.L., 1977. High-temperature creep of Mt. Burnet Dunite. *Tectonophysics*, 42: 75–110.
- Rutter, E.H., 1970. *An Experimental Study of the Factors Affecting the Rheological Properties of Rock in Simulated Geological Environments*. Thesis. Imperial College, London.
- Rutter, E.H., 1974. The influence of temperature, strain rate and interstitial water in the experimental deformation of calcite rocks. *Tectonophysics*, 22: 311–334.

- Schmid, S.M., 1976. Rheological evidence for changes in the deformation mechanism of Solnhofen limestone towards low stresses. *Tectonophysics*, 31: T21—T28.
- Schmid, S.M., Boland, J.N. and Paterson, M.S., 1977. Superplastic flow in finegrained limestone. *Tectonophysics*, 43: 257—291.
- Turner, F.J. and Heard, H.C., 1965. Deformation of calcite crystals at different strain rates. *Geol. Sci. Publ., Univ. of California, Los Angeles*, 46: 103—126.
- Twiss, R.J., 1977. Theory and applicability of a recrystallized grain size paleopiezometer. In: M. Wyss (Editor), *Stress in the Earth*. Reprint from *Pageoph.*, 115, in *CCRG*, 3: 227—244, Birkhäuser Verlag, Basel.
- Weertman, J., 1975. High temperature creep produced by dislocation motion. In: J.C.M. Li and A.K. Mukherjee (Editors), *Rate Processes in Plastic Deformation of Materials*. ASM, Metals Park, Ohio, pp. 315—336.